JOURNAL OF MATERIALS SCIENCE 32 (1997) 5419–5423

Mapping of residual stresses around an indentation in β-Si_3N_4 using Raman spectroscopy

N. MURAKI, G. KATAGIRI
Materials Science Laboratory, Toray Research Center, Inc., Sonoyama, Otsu, Shiga 520, Japan

V. SERGO
Materials Engineering and Applied Chemistry Department, University of Trieste, Via Valerio, Trieste 34127, Italy

G. PEZZOTTI, T. NISHIDA
Department of Materials, Kyoto Institute of Technology, Matsugasaki, Kyoto 606, Japan

The stress dependence of the Raman bands of silicon nitride (β-Si_3N_4) have been investigated and applied to indentation experiments. Seven high-frequency bands have been found to have linear and negative stress dependencies. On the other hand, low frequency bands (namely 183, 205 and 226 cm^{-1} bands) showed small positive correlations with the stress. The piezospectroscopic (PS) coefficients of all the observed Raman bands have been determined. As an application, one of the PS coefficients has been used to determine the stress distribution around a triangular indentation.

1. Introduction

In recent years, several papers have been published that deal with the determination of residual or applied stresses in ceramic materials using spectroscopic techniques [1–7]. The general method, henceforth called PS, utilizes the relation between the Raman or fluorescence band frequency and the stress. Usually, for small strains the band peak frequencies have a linear correlation with the stress, the slope being called the PS coefficient. The residual stresses in the material of interest are obtained from a knowledge of the stress-induced shift of the band position and the PS coefficient. The PS method presents many advantages:

1. non-destructive and non-contact evaluation;
2. micrometre spatial resolution (using an optical microprobe);
3. a short measurement time and
4. stresses into the individual phases constituting a composite material can be derived.

However, until now, this method has been applied only in a limited number of materials (e.g. Al_2O_3 [1–7], Si [8–10], graphite [11, 12] and some others (13, 14]). The main reason for the restriction is due to the rather low intensities of the Raman bands of most ceramics. Al_2O_3 is a fortutious case, in that it exploits the fluorescence due to chromium impurities.

Silicon nitride (Si_3N_4) is an important structural ceramic material, widely used as a monolith as well as a matrix for ceramic composites. In a previous report, Sergo *et al.* [15], presented the stress dependencies of the Raman spectra of β-Si_3N_4 with different sintering additives. In this contribution we present a practical application of those results, i.e. the measurement of the residual stresses surrounding a Berkovich indentation.

The first step in PS analysis of applied or residual stresses is the determination of the PS coefficient of the material of interest. Given the non-negligible dependencies of the PS coefficients on the additives and sintering conditions [15], a new calibration has been performed before determining the stress around the indentation. For this work, the PS coefficients have been determined for most of the observed Raman bands of β-Si_3N_4. A suitable band has been used to determine the stress distribution around a triangular indentation.

1.1. PS analysis

In a first-order approximation, the stress dependence of a Raman band position is governed by the following tensorial expression:

$$\Delta\nu = \Pi_{ij}\sigma_{ij} \quad (1)$$

where $\Delta\nu$ is the peak frequency shift, σ_{ij} is the stress tensor and Π_{ij} is the matrix of the PS coefficients. This equation is correct for stresses applied in the crystallographic reference frame of the material under investigation. For the more general case of a stress tensor randomly orientated, a transformation matrix is required. In the case of polycrystalline samples, the tensor expression loses its meaning. In this case, the measured frequency shift of the stressed material, $\langle\Delta\nu\rangle$, can be expressed by the relationship

$$\langle\Delta\nu\rangle = \Pi_{tr}\langle\sigma_i\rangle \quad (2)$$

where Π_{tr} is the trace of the PS tensor and $\langle \sigma_i \rangle$ is the mean stress. If a uniaxial stress, $\langle \sigma_{uni} \rangle$, is applied to a polycrystalline substance, the relationship can be expressed using an average of the diagonal PS tensor, $\Pi_{ave} = \Pi_{tr}/3$

$$\langle \Delta\nu \rangle = \Pi_{ave} \langle \sigma_{uni} \rangle \quad (3)$$

As far as the calibration tests in four-point bending system are concerned, applied stresses at the centre of the sample can be regarded as uniaxial and changing linearly from compression to tension. Hence, Equation 3 can be used and the average PS coefficients, Π_{ave}, are determined.

2. Experimental procedures

2.1. Material

High purity Si_3N_4 powder (E-10, Ube Ind. Ltd, Ube, Japan) without addition of sintering aids was used as the raw material. Hot-isostatically pressing (HIP) sintering was performed after encapsulating the specimen into a borosilicate glass tube (evacuated to 0.1 Pa). The HIP cycle was conducted in an argon atmosphere under a pressure of 180 MPa for 2 h at 1950 °C. The specimen was fully dense (99.5%) and oxygen analysis, performed on the sintered body, revealed an SiO_2 content of about 2.4 wt%. SiO_2 is a natural impurity that originated from the surface oxidation of the starting Si_3N_4 powder. The impurity content in the sintered body was determined by an inductively coupled radio-frequency Plasma emission spectrometer (ICP); the total amount of cation impurities, as detected in the sintered body, was less than 200 p.p.m. wt. The sintered sample was cut in the shape of bars ($3 \times 4 \times 50$ mm); one 4×50 mm side was polished with fine diamond paste (1 μm) and the specimen was annealed for 3 h at 1400 °C. The bars were mounted on a four-point bend jig that was specially made for the calibration test of the stress dependence, and the applied load was obtained from a load cell in contact with the jig. The four-point bending system has the advantage of providing a uniform distribution of stress in the region of the upper span, as compared with the three-point bending system. The load was converted to stress by means of the four-point elastic beam bending equation. A Berkovich indenter (MCTE-500, Shimadzu Co.) with a load of 5 N was used to form the triangular indentation.

2.2. Raman spectroscopy

An argon ion laser operating at a wavelength of 488.0 nm with a power of 50 mW on the sample was used as the excitation source. In the case of the calibration experiments, the exciting laser was focused onto the samples with an optical lens and a small mirror (back scattering mode). The size of the probe beam on the sample was about 100 μm. A camera lens was used to collect the scattered light, which was then analysed with a monochromator; the single monochromator option was employed, equipped with a CCD camera (T-64000 Jobin-Yvon, ISA). After the load was applied, a spectrum was recorded every 200 μm step from the compressive side to the tensile side of the bend bar. The polarization of the incident light was parallel to the direction of uniaxial stress. Instrumental fluctuations were compensated for by monitoring the spectrum from a neon discharge lamp (503.77 nm line that corresponded to a 642.250 cm^{-1} Raman shift in the case of 488.0 nm excitation).

An optical microprobe was used for the measurement of the stress distribution around the triangular indentation. The exciting laser was focused onto the sample with an optical microscope, and the same objective lens ($\times 100$) was used to collect the scattered light. The scattered light passed through the cross slit, which rejected the light from the defocusing region. The effective depth of the microprobe measurement can be changed roughly by the dimension of the cross slit. In the present work, the cross slit was 400 μm and the effective measurement depth was about ~ 5 μm. The dimension of the laser spot on the sample was about ~ 2 μm. The laser irradiation time was $\sim$ about 60 s per spectrum. (Preliminary experiments showed that there were no shifts of the peaks due to laser heating.)

The recorded spectra were manipulated with commercially available software (Grams/386, Galactic Ind. Co.). In order to obtain the peak frequency of each Raman band, all the Raman bands were curve-fitted to a mixture of Lorenzian and Gaussian functions.

3. Results and discussion

3.1. Calibration: stress dependence of the Raman bands

Fig. 1 shows the Raman spectrum of the HIP Si_3N_4 under investigation. The most intense Raman band, at about 520 cm^{-1}, was assigned to pure elemental silicon, probably derived from the thermal decomposition of Si_3N_4 [16–18]

$$Si_3N_4 \rightarrow 3Si + 2N_2 \quad (4)$$

Although the observed bands of β-Si_3N_4 have not been completely assigned to symmetry modes, rather

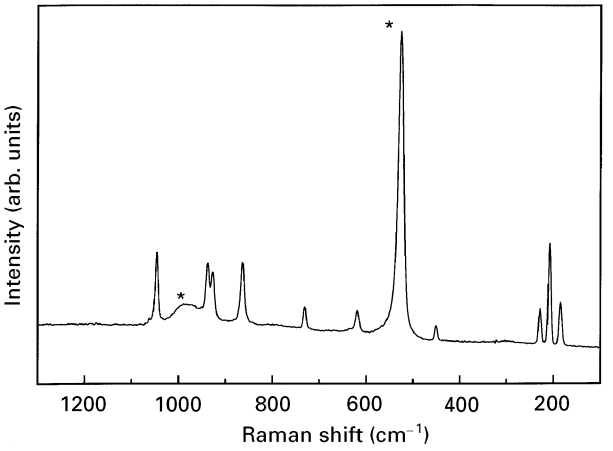

Figure 1 Raman spectra of the sintered Si_3N_4 material under investigation. There are 11 Raman bands that are assigned to β-Si_3N_4. (*) bands for free Si deriving from the thermal decomposition of Si_3N_4 during HIP.

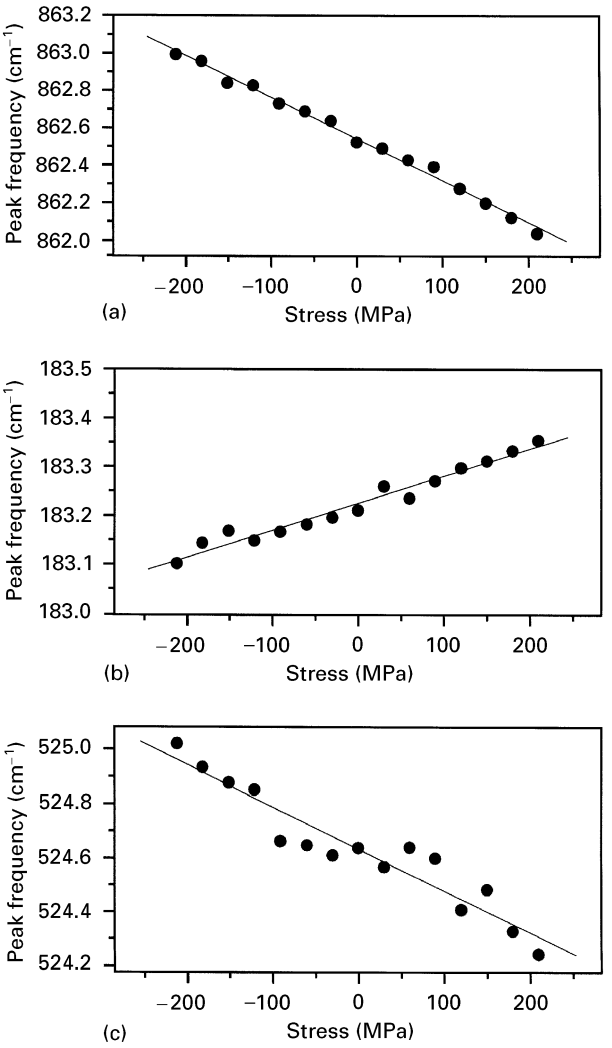

Figure 2 Stress dependencies of the positions of some band: (a) 862 cm^{-1}, (b) 183 cm^{-1}, and (c) the free Si band at 524 cm^{-1}. Note the opposite stress dependence of the low frequency mode at 182 cm^{-1}, likely because this is an external vibrational model.

intense and sharp Raman bands around 200 cm^{-1} (183, 205 and 226 cm^{-1}) were assigned to the lattice vibrational modes [19, 20]. The other bands in the region between 300 and 1200 cm^{-1} were assigned to the internal modes [19, 20].

As an example, the stress dependence of the band at 862 cm^{-1} from -200 to $+200$ MPa is shown in Fig. 2. The slope of the linear least square fit has been assumed to be the PS coefficient. Depending on the convention assumed for the slope of the shift of the band position, the PS coefficient assumes different signs: here, $\Delta\nu$ is the difference between the stressed and the unstressed band position. The stress dependences of the band positions at 183 and 526 cm^{-1} are also displayed in Fig. 2. The latter is the band of elemental silicon and its peak frequency is known to have a well defined stress dependence [8, 9]. Improved stability of the Raman acquisition system has enabled a more accurate stress dependence of the silicon band, which was precluded in a previous contribution [15]. According to the experiments from hydrostatic studies [10], the uniaxial stress dependence of the peak position of the 520 cm^{-1} band results at $-1.73\,cm^{-1}\,GPa^{-1}$; our value is $-1.55\,cm^{-1}\,GPa^{-1}$.

TABLE I Experimental results of stress dependence of the Raman band of sintered β-Si_3N_4. For each band the peak frequency; the width; the PS coefficient, Π; and the correlation coefficient of least square fit, *R*; are shown

Peak frequency (cm^{-1})	Band width (cm^{-1})	Π ($cm^{-1}\,GPa^{-1}$)	*R*
183.23	4.20	0.56 ± 0.013	0.982
206.08	3.70	0.26 ± 0.029	0.984
226.75	3.80	0.27 ± 0.021	0.962
448.92	4.10	-0.51 ± 0.059	−0.923
524.63[a]	12.04	-1.55 ± 0.13	−0.900
617.62	6.57	-1.15 ± 0.089	−0.962
729.65	4.79	-0.99 ± 0.067	−0.972
862.54	7.12	-2.22 ± 0.051	−0.997
926.51	7.07	-2.15 ± 0.076	−0.992
937.32	6.33	-2.08 ± 0.088	−0.989
1044.91	5.64	-1.89 ± 0.054	−0.994

[a] Free Si peak.

Therefore, elemental Si in the sintered Si_3N_4, although we do not have *a priori* knowledge about its location, must be subjected to the same influence of applied stress as the matrix Si_3N_4 [21]. Equation 4 would yield silicon only partially bonded to the Si_3N_4 lattice and this possibly explains the weaker stress dependence compared with the literature value. The reason for the rather large deviation of the peak position may reside in the inhomogeneity of the residual stress of Si or the distribution of the Si grain size.

All the monitored PS coefficients are summarized in Table I. The PS coefficients of Si_3N_4 are positive for the triplet mode around 200 cm^{-1}, and this further confirms the hypothesis that these bands are due to external vibrational modes [19, 20]. The largest absolute PS coefficient, 2.22 $cm^{-1}\,GPa^{-1}$, belongs to the band at 862 cm^{-1}, which is thus most suitable for subsequent application.

As far as the band widths are concerned, it is confirmed [15] that in the stress region under investigation (-200 to $+200$ MPa), no obvious correlation was found in all the bands under observation.

3.2. Application: residual stress distribution around a triangular indentation

Fig. 3a shows a scanning confocal laser micrograph of the triangular indentation, and its pseudo three-dimensional map is shown in Fig. 3b. The side length of the indented area is about 20 μm and the maximum depth is 2 μm. Limited swelling can be seen just around the edge of the indentation. Raman measurements have been taken along lines A and B indicated in Fig. 3a. No crack could be detected at the corner of the indented area by the present resolution.

The peak shifts of the 862 cm^{-1} band have been converted to stress and the stress distribution around the indentation is shown in Fig. 4. The stress is compressive around the indentation centre and the maximum compressive stress is nearly 1 GPa located at about 10 μm from the indentation centre. Although the shape of the indentation is not the same along lines

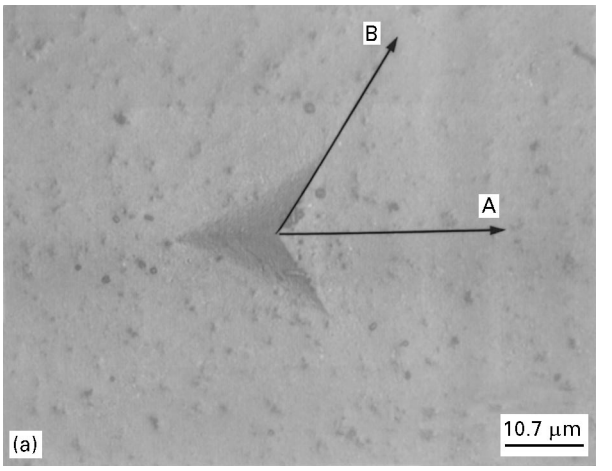

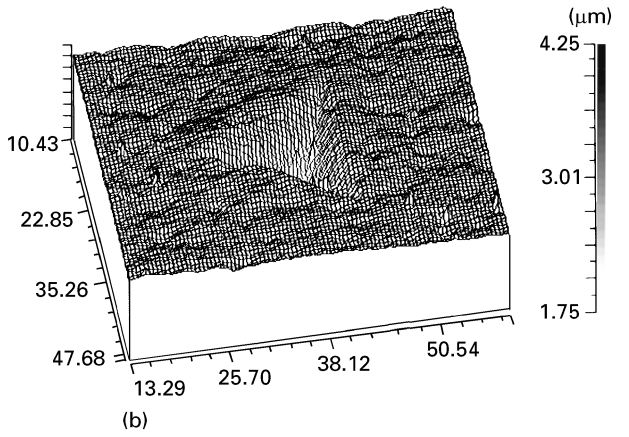

Figure 3 Results of observation by confocal scanning laser microscope: (a) micrograph of a micrometre-sized indentation, Raman microprobe measurements were performed both along the line A and B; and (b) three-dimensional display of the indentation, it shows that there is some swelling of the material around the indentation side.

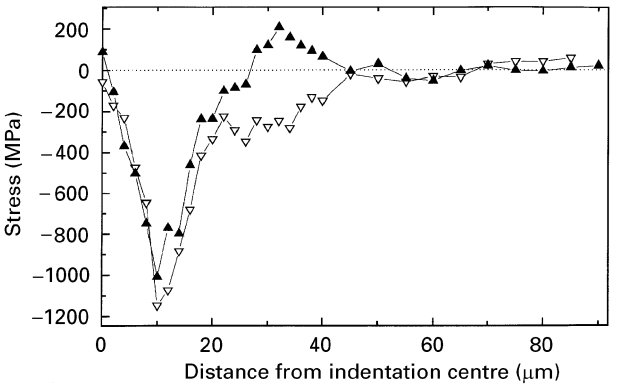

Figure 4 Residual stress distribution around a triangular indentation: (▽) stress along line A (cf. Fig. 3), (▲) stress along line B. The error involved in the measurement is the same order of the dimension of the triangular dots.

A and B, the stress behaviour is quite similar from the centre to a distance of about 25 μm from it, which leads to the conclusion of a circular symmetry of stress in this area. Outside this region, the zero stress level is reached almost monotonically along line A. Along line B, in the region from 25 to 45 μm, a tensile stress with a maximum of 200 MPa is detected. This phenomenon

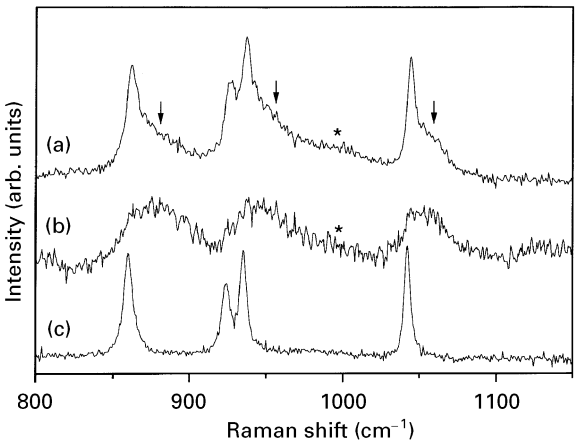

Figure 5 High-frequency region spectra: (a) at the indentation centre; (b) at the same position with a confocal configuration, and (c) far away from the indentation with a confocal configuration. Spectrum (a) clearly shows a high frequency shoulder that has been attributed to an amorphous or heavily distorted layer. Spectrum (b) confirms that this layer is located at the surface of the indentation, and there is no broad band away from the indentation (c). (∗) broad band of free Si.

can be explained by considering the shape of the indentation: during indentation, three faces of the tetrahedral indenter push the material perpendicularly to their respective planes, and hence, for equilibrium, a tensile stress is induced along the direction of the indentation corner and perpendicular to it. This is the stress that generally induces small cracks whose lengths are used for empirically measuring toughness in engineering ceramics [22].

As shown in Fig. 4, the stress at the indentation centre is apparently close to zero, this datum is not trivial and might be related to another interesting feature; the formation of an amorphous or heavily distorted surface layer in the area below the centre of the indenter. This phenomenon is discussed hereafter.

Fig. 5 shows the Raman spectra taken at the indentation centre (Fig. 5a), at the same position but measured in the confocal configuration (Fig. 5b), and at a point well away from the indentation in the confocal configuration (Fig. 5c). In the spectrum of the indentation centre, a much broader and high-frequency shifted band can be observed in addition to the sharp bands. This broader band, which is similar to a glassy phase band [23], may be attributed to plastic deformation. In this region, the structure of the Si_3N_4 crystal lattice has probably been damaged by the compressive stress and, as a consequence, an amorphous or heavily flouted layer has formed at the specimen surface. The confocal measurement was performed by using a cross slit (the slit width was 50 μm), and the effective measurement depth was only about 1 μm. Only high frequency broad bands are seen in Fig. 5b, therefore, lattice amorphism or heavy distortion might have occurred at the surface of the indentation. At present, PS analysis can only measure elastic residual stresses, while the assessment of plastic deformation, as seen in the centre region of the indentation, is beyond its ability. In our analysis of residual stress distribution, the broader side band was included in the

curve-fitting calculation. Therefore, the value of the residual stress beneath the indentation centre may have been more tensile than the real value.

4. Conclusions

The stress distribution around a micrometre-sized triangular indentation in β-Si_3N_4 has been experimentally determined by PS. To obtain the stress value precisely the dependencies of ten Raman bands of dense, high purity Si_3N_4 have been determined. The present study shows the possibility of obtaining precise stress information on the micrometre scale in Si_3N_4 materials and, hence, provides the basis for a detail microstructural analysis of this important structural material.

References

1. S. E. MOLIS and D. R. CLARKE, *J. Amer. Ceram. Soc.* **73** (1990) 3189.
2. Q. MA, and D. R. CLARKE, *Acta Metall. Mater.* **41** (1993) 1817.
3. Q. MA, W. POMPE, J. D. FRENCH and D. R. CLARKE, *ibid.* **42** (1994) 1673.
4. Q. MA, L. C. LIANG D. R. CLARKE and J.W. HUTCHINSON, *ibid.* **42** (1994) 3299.
5. Q. MA and D. R. CLARKE, *J. Amer. Ceram. Soc.* **77** (1994) 298.
6. *Idem*, *ibid.* **76** (1993) 1433.
7. V. SERGO, D. R. CLARKE and W. POMPE, *ibid.* **78** (1995) 633.
8. I. DE WOLF, J. VANHELLEMONT, A ROMANO-RODRIGUEZ H. NORSTROEM and H. E. MAES, *J. Appl. Phys.* **71** (1992) 898.
9. M. YOSHIKAWA M. MAEGAWA, G. KATAGIRI and H. ISHIDA, *ibid.* **78** (1995) 941.
10. B. A. WEINSTEIN and G. J. PIERMARINI, *Phys. Rev.* **B12** (1975) 1172.
11. L. S. SCHADLER, C. LAIRD, N. MELANITIS, C. GALIOTIS and J. C. FIGUEROA, *J. Mater. Sci.* **27** (1992) 1663.
12. N. MELANITIS and C. GALIOTIS, *ibid.* **25** (1990) 5081.
13. J. F. DIGREGONIRIO, T. E. FURTAK and J. J. PETROVIC, *J. Appl. Phys.* **71** (1992) 3525.
14. C. VALTTAS and C. GALIOTIS, *Polymer* **35** (1994) 2335.
15. V. SERGO, G. PEZZOTTI, G. KATAGIRI, N. MURAKI and T. NISHIDA, *J. Amer. Ceram. Soc.* in press.
16. H. D. BATHA and E. D. WHITNEY, *ibid.* **56** (1973) 365.
17. C. C. GRESKOVICH and S. PROCHAZKA, *ibid.* **64** (1981) C96.
18. C. GRESKOVICH, *ibid.* **64** (1981) 725.
19. A. TAKASE and E. TANI, *J. Mater. Sci. Lett.* **6** (1987) 607.
20. N. WADA, S. A. SOLIN, J. WONG and S. PROCHAZKA, *J. Non-Cryst. Solids* **43** (1981) 7.
21. D. R. CLARKE, *Mater. Sci. Forum* **47** (1989) 110.
22. G. R. ANSTIS, P. CHANTIKUL, B. R. LAWN and D. B. MARSHALL, *J. Amer. Ceram. Soc.* **64** (1981) 533.
23. A. JAYARAMAN, G. A. KOUROUKLIS, A. S. COOPER and G. P. ESPINOSA, *J. Phys. Chem.* **94** (1990) 1091.

Received 19 April 1996
and accepted 2 April 1997